ADVANCED FUNCTIONAL MATERIALS
www.afm-journal.de

A Clear, Strong, and Thermally Insulated Transparent Wood for Energy Efficient Windows

*Ruiyu Mi, Tian Li, Daniel Dalgo, Chaoji Chen, Yudi Kuang, Shuaiming He, Xinpeng Zhao, Weiqi Xie, Wentao Gan, Junyong Zhu, Jelena Srebric, Ronggui Yang, and Liangbing Hu**

The energy used for regulating building temperatures accounts for 14% of the primary energy consumed in the U.S. One-quarter of this energy is leaked through inefficient glass windows in cold weather. The development of transparent composites could potentially provide affordable window materials with enhanced energy efficiency. Transparent wood as a promising material has presented desirable performances in thermal and light management. In this work, the performance of transparent wood is optimized toward an energy efficient window material that possesses the following attributes: 1) high optical transmittance (≈91%), comparable to that of glass; 2) high clarity with low haze (≈15%); 3) high toughness (3.03 MJ m^{-3}) that is 3 orders of magnitude higher than standard glass (0.003 MJ m^{-3}); 4) low thermal conductivity (0.19 W m^{-1} K^{-1}) that is more than 5 times lower than that of glass. Additionally, the transparent wood is a sustainable material, with low carbon emissions and scaling capabilities due to its compatibility with industry-adopted rotary cutting methods. The scalable, high clarity, transparent wood demonstrated in current work can potentially be employed as energy efficient and sustainable windows for significant environmental and economic benefits.

1. Introduction

The building sector consumes ≈40% of the total energy in the United States.[1,2] Residential building windows in particular account for 10–25% of the heat loss due to their poor thermal management capability,[3] with ≈3.95 quads (or 1.16 × 10^{12} kWh) of primary energy consumed through windows in cold weather.[4] At present, glass is considered as the most commonly used window material. However, single-pane glass windows suffer from the following weaknesses. First, glass has a high intrinsic thermal conductivity (≈1 W m^{-1} K^{-1}), leading the energy required for heating to easily leak.[5] Second, glass is fragile and tends to break upon sudden impact, making it a safety hazard.[6] Moreover, massive CO_2 emissions of 25 000 metric tons per year are produced during glass production.[7] Exploring energy efficient window materials is thus highly desirable to address heating costs, energy shortages, and the global impact of climate change associated with increased carbon emissions.

To address these issues, several technologies have been developed, including internal and external blinds,[8] transparent thermal barriers,[9] angular selective shading systems,[10] coatings,[11] films,[12] and multipane windows.[13] The development of transparent wood as an alternative transparent material has aroused wide attentions.[6,14–21] L. Berglund's group used sodium chlorite ($NaClO_2$) method to bleach the natural wood and infiltrated polymethyl mechacrylate (PMMA) to obtain transparent wood.[6,22] Hu's group adopted a two-step solution-proceed strategy to remove lignin and fabricate transparent wood via the epoxy impregnation.[15,16] The transmittance achieved is about 90%. However, challenges remain including reducing haze, enhancing mechanical properties, and thermal insulation for energy efficient windows.

Here, we developed the transparent wood composite with simultaneously optimized optical properties, thermal insulation, and mechanical properties (**Figure 1**b). This work largely improved the performance of transparent wood toward realistic applications of energy efficient windows. In our process, first, a prolonged sodium hypochlorite (NaClO) bleaching process was utilized to completely remove lignin and most of hemicellulose, yielding nanoscale cellulose fibers with a diameter smaller than the wavelengths of visible light. Furthermore, polyvinyl alcohol (PVA) with strong hydrogen bonding and a highly matched optical refractive index[23] was infiltrated into the porous

R. Mi, Dr. T. Li, C. Chen, Y. Kuang, S. He, W. Xie, W. Gan, Prof. L. Hu
Department of Materials Science and Engineering
University of Maryland
College Park, MD 20742, USA
E-mail: binghu@umd.edu
D. Dalgo, Prof. J. Srebric
Department of Mechanical Engineering
University of Maryland
College Park, MD 20742, USA
X. Zhao, Prof. R. Yang
Department of Mechanical Engineering
University of Colorado
Boulder, CO 80309, USA
J. Zhu
Forest Products Laboratory
USDA Forest Service
Madison, WI 53726, USA
The ORCID identification number(s) for the author(s) of this article can be found under https://doi.org/10.1002/adfm.201907511.

DOI: 10.1002/adfm.201907511

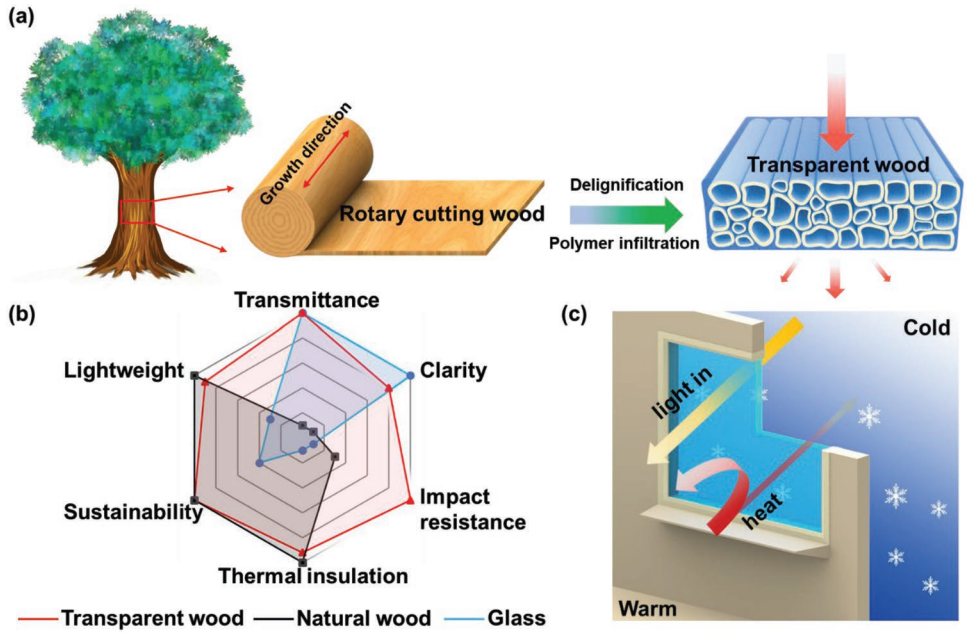

Figure 1. Schematic illustration of the fabrication process of the transparent wood, which features various outstanding characteristics compared to glass windows. a) The large-scale naturally aligned wood is obtained by a scalable industry-adopted rotary cutting method. The transparent wood features optimized optical properties after delignification and PVA infiltration. b) A radar chart compares the various properties of the transparent wood, natural wood, and glass when used as building materials. c) A schematic of the energy saving process while using the transparent wood in the exterior windows of a building in cold weather.

cellulose scaffold, resulting in the formation of a dense structure. Specifically, the developed transparent wood is ≈3 times stronger (high tensile strength of 143 ± 17.5 MPa) than the previous reported value.[16] Consequently, compared with other transparent wood reported in previous studies (>80%), a lower optical haze (≈15%) is obtained.[15,21,24] In addition, the thermal conductivity of the transparent wood (0.19 W m^{-1} K^{-1}) is greatly reduced,[14,25] which is about 5 times lower than typical glass (≈1 W m^{-1} K^{-1}).[5] In addition, the wood veneer used to synthesize transparent wood is cut by a rotary cutting method, which is a large-scale fabrication technique already compatible with industry (Figure 1a). Due to the combination of these outstanding merits, particularly the high clarity, enhanced mechanical properties, and effective thermal insulation, our developed transparent wood has great potential to replace glass as a promising energy-efficient building material (Figure 1b,c).

2. Results and Discussion

Balsa is the lowest density tree species, largely due to its fast growth,[26] and appears opaque due to the absorbance of light by lignin[27] (one of the primary components of wood, containing chromophores with a refractive index of 1.61) and scattering between the microsized cell walls.[19,28] To fabricate transparent wood with high clarity, we immersed the wood in NaClO solution at room temperature to remove the light absorbing substances from the wood structure. **Figure 2**a shows the 3D mesoporous natural balsa wood structure, which features long microchannels that are not uniform in diameter, ranging from 20 µm to 400 µm[29] (Figures S1 and S2, Supporting Information). After the prolonged bleaching process, the wood structure becomes more porous with dramatically thinner wood cell walls (≈0.5 µm) compared to that of the original wood (≈3.5 µm) (Figure 2b,c). However, the overall delignified wood still features a well-preserved morphological structure at the microscale. To further confirm the effect of the bleaching process, the chemical composition analysis of natural wood and delignified wood are carried out as indicated in Figure S3 in the Supporting Information. Most specifically, natural wood is mainly composed of 38.57% cellulose, 12.95% hemicellulose, and 20.3% lignin. There shows a large enhancement on the cellulose content to 60.6%, while the contents of hemicellulose and lignin have decreased to 4.99% and 0.8% after the delignification using NaClO. Consequently, the delignified wood exhibits a minimized light absorption and an increased transmission in the visible spectral range (Figure S4, Supporting Information) due to the removal of lignin. Then in order to obtain high optical transmittance and low haze simultaneously, we infiltrated the wood template with PVA (see the Experimental Section). PVA is widely used in composites as it is an environmentally friendly polymer featuring optical transparency.[30–32] Additionally, PVA has good wettability on cellulose and a well-matched refractive index ($n \approx 1.53$–1.54)[23] with cellulose and hemicellulose ($n = 1.53$).[33] Figure 2d shows a photo of the resulting transparent wood after polymer infiltration, through which the textures of the leaf can be clearly seen. As illustrated in Figure 2e,f, high transparency is made possible by the full permeation of the polymer in the delignified wood structure. The infiltration of PVA into the wood scaffold may result in effective hydrogen bonding between PVA and cellulose, leading to the formation of a tightly packed

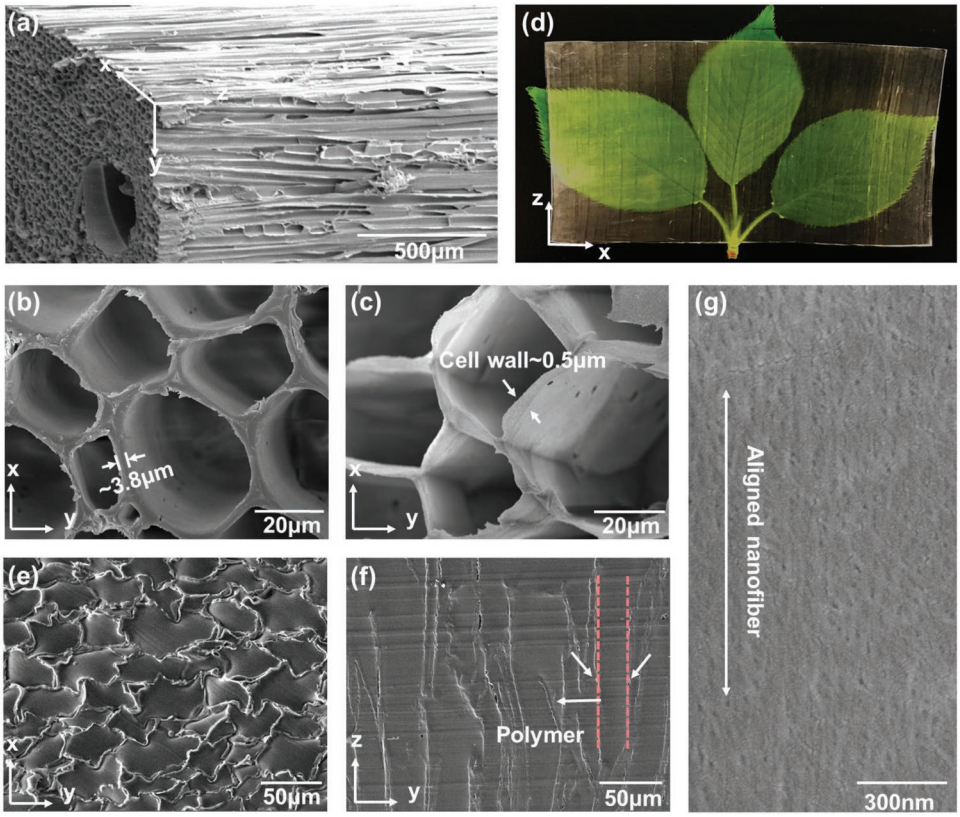

Figure 2. Characterization of the transparent wood microstructure. a) Scanning electron microscopy (SEM) image of the 3D mesoporous balsa wood. Top view SEM images of the b) natural wood and c) delignified wood, showing the thinner wood cell walls after the delignification process. d) Photo of the obtained transparent wood (100 mm × 50 mm × 0.8 mm) with high transmittance and low haze. e,f) SEM images of the polymer-filled transparent wood, showing the dense wood structure. g) Magnified view of the microsized channel walls, in which aligned nanocellulose fibers can be observed.

composite structure (Figure 2g; Figure S5, Supporting Information).[34] To quantify the influence of the NaClO treatment time on the optical properties of the obtained transparent wood, we measured the haze spectra of transparent wood samples assembled at different bleaching times (Figure S6, Supporting Information). Our results show that as the treatment time was increased from 3 to 24 h, the corresponding haze was tailored from 87% to 15%. These findings suggest that excessively bleaching the wood template may expose a greater number of nanocellulose fibers,[21] causing lower light scattering in the resulting transparent wood. The prolonged delignification treatment of the natural wood, as well as the refractive index well-matched infiltrating polymer drastically reduces the transparent wood's optical scattering, leading to a desirable combination of high transmittance and low haze.

The anisotropic structure also leads to remarkable anisotropic light management performance. As shown in the schematic of **Figure 3**a, the oriented nanostructures in the sample can be observed distinctly when their alignment direction (marked by the black arrows) is similar to that of the optical polarizer (Figure 3b). The ability to control the optical transmittance of the material with different polarization due to the alignment of the cellulose fibers confirms that the anisotropic structure has potential for light management applications. In addition, the densely packed transparent wood with its longitudinally aligned channels presents minor light scattering. We applied a 532 nm laser source with a spot size of 200 μm to irradiate our transparent wood, using a detector behind the sample to record the intensity profile of the transmitted light. The transmittance scattering presents an anisotropic pattern, but with a small divergence. Angular distributions of the transmitted light scattering in the *x*- and *y*-directions are shown in Figure 3c, in which the cellulose fibers are aligned in the *y*-direction, leading to a larger optical divergence in the *x*-direction. In addition, the maximum scattering angle can be used to reveal the extent of light scattering in the low haze transparent wood. The maximum scattering angle was calculated to be 12.4°, which results from the densely packed cellulose nanofibers, similar to the scattering mechanism of previously reported clear paper.[35,36] Figure 3d further demonstrates the unprecedented combination of high transmittance (≈91%) and low haze (≈15%) in the transparent wood while the pure polymer exhibits transmittance (≈92%) and haze (≈6%). Figure 3e and Table S1 in the Supporting Information summarize and compare our work with other transparent wood obtained by different processes and wood species.[6,15,16,21,22,25,29,37] As can be seen, our work realized the lower optical haze among the previous transparent wood works. Moreover, a desirable feature for window materials is the blockage of ultraviolet light, as it can accelerate the deterioration of room furnishings, as well as cause health problems, including skin cancer and eye damage.[38] As illustrated in

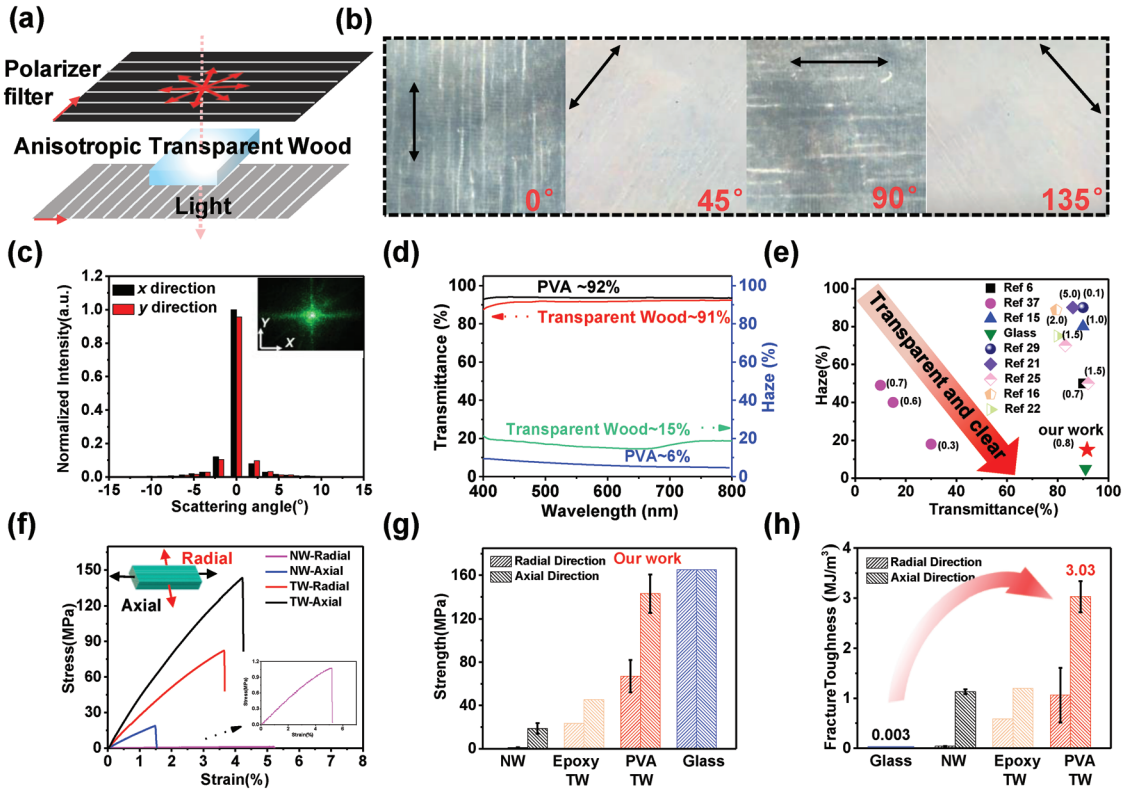

Figure 3. Optical and mechanical characterization of the transparent wood. a) Schematic illustration of the anisotropic transparent wood between crossed polarizers. b) The polarization effect of the samples. The black arrow shows the cellulose fiber alignment direction. c) The normalized scattered light intensity distribution in the *x*- and *y*-directions, indicating the transparent wood's anisotropic optical transmittance. The inset shows a photo of the scattered light spot. d) Optical properties of pure polymer (PVA) and our transparent wood (0.8 mm). e) Optical haze versus transmittance of our transparent wood and other transparent wood prepared by different processes and wood species.[6,15,16,21,22,25,29,37] f) Experimental stress–strain curves of natural wood (NW) and our transparent wood (TW) in radial and axial directions. g,h) Strength and toughness comparison between natural wood, epoxy transparent wood,[16] glass,[14] and our PVA transparent wood.

Figure S7 in the Supporting Information, our transparent wood can shield 100% of UVC wavelengths (200–275 nm) and more UVB (275–320 nm) light compared to glass of the same high transmittance in the visible light range.

Apart from the unique optical properties, our demonstrated transparent wood also exhibits improved mechanical performance (Figure 3f–h). In terms of glass, it is extremely brittle which features potential safety concerns, although it is widely used in building construction. In contrast, our transparent wood can sustain stronger impact mainly due to the dense wood structure formed by the combination of cellulose and the energy absorbing polymer filler. Figure 3f,g displays the tensile-strain curves of the natural wood and transparent wood in radial and axial directions, in which the applied stress parallel to the wood channel direction is axial direction and perpendicular to the wood channel is radial direction (as schematically shown in the inset of Figure 3f). The transparent wood features a significantly higher tensile strength of 143 ± 17.5 MPa in axial direction while exhibits 67 ± 15 MPa in radial direction. Note that the mechanical properties are improved in both axial direction and radial direction, compared to the natural balsa wood (18.8 ± 4.9 MPa, 1.15 ± 0.347 MPa) and transparent wood fabricated by infiltrating epoxy (45.4 MPa, 23.38 MPa),[16] due to the effective hydrogen bonding between PVA and the nanocellulose fibers.[39] Although the strength of glass[14] is a little higher than our transparent wood, it bears a lower degree of stress and tends to fail suddenly when it suffers a load.[40] That is, our transparent wood (3.03 ± 0.31 MJ m^{-3}) possesses a much higher fracture toughness than standard glass (0.003 MJ m^{-3}),[14] natural wood (0.14 ± 0.06 MJ m^{-3}), and epoxy transparent wood (1.2 MJ m^{-3}; Figure 3h)[16] in axial direction. In addition, the mechanical properties including tensile strength, modulus, and toughness of as-prepared transparent wood and natural wood in radial and axial directions are summarized in Table S2 in the Supporting Information. Consequently, the dramatic improvement in the ductility makes our transparent wood desirable for application as a building material, mitigating safety risks as it fails by bending or splitting without producing sharp pieces.

In conventional single-pane window systems, typical glass possesses a high thermal conductivity (≈1 W m^{-1} K^{-1}), which adversely impacts building energy efficiencies. Therefore, to develop efficient alternatives to glass windows, in addition to the optical and mechanical requirements that have already been discussed, another important issue is the material's thermal insulation capability. In this study, the designed transparent wood with lower thermal conductivity can efficiently prevent heat dissipation. **Figure 4**a shows the anisotropic thermal conduction of the transparent wood. Along the radial direction

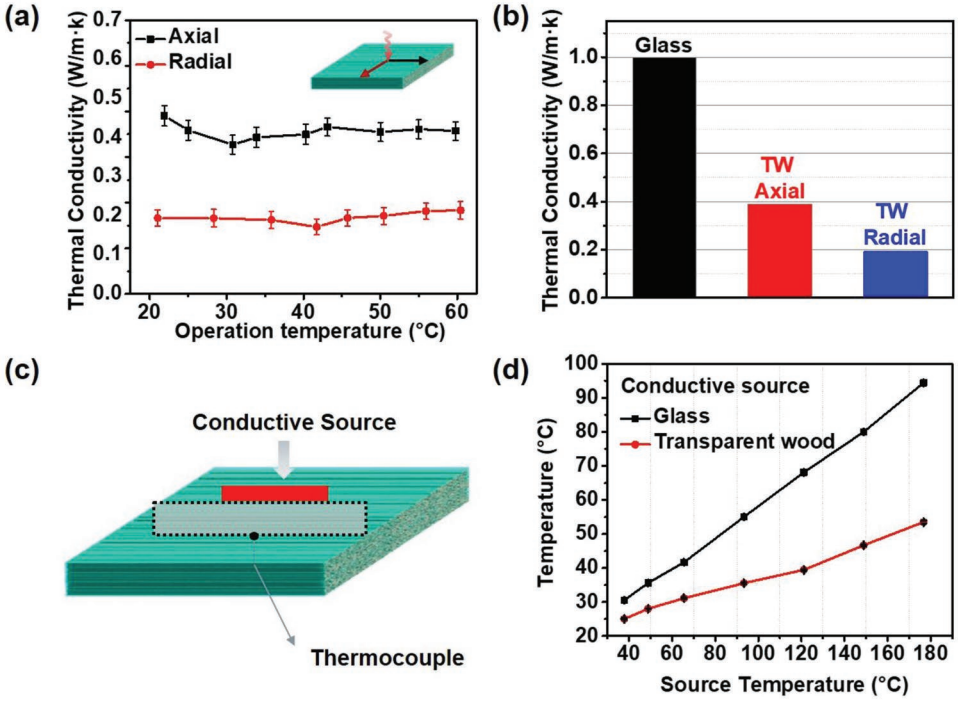

Figure 4. Thermal insulation performance of transparent wood comparing with glass. a) The thermal conductivity of the transparent wood was measured from 20 to 60 °C at the axial and radial heat transfer directions. b) Comparison of the thermal conductivities of standard glass and the axial and radial directions of the transparent wood. c) The schematic of the transparent wood being heated transversely (perpendicular to the wood fibers). d) The stable backside temperatures of the glass and transparent wood samples after the top surfaces had been directly contacted with a conductive heat source via thermal paste at different temperatures.

(i.e., perpendicular to the aligned nanocellulose fibers), the heat transfer is confined while thermal energy is conducted mostly in the axial direction due to the orientation of the nanofibers.[41] Laser flash apparatus (LFA) measurements reveal that the thermal conductivity slightly varies from room temperature to 60 °C. The thermal conductivity is 0.19 ± 0.020 W m^{-1} K^{-1} at room temperature in the radial direction, while it slowly changes from 0.39 ± 0.022 W m^{-1} K^{-1} at 21.9 °C to 0.357 ± 0.020 W m^{-1} K^{-1} at 59.8 °C in the axial direction. This means the thermal energy tends to spread in the direction parallel with the wood channels compared to the radial direction, as shown in the infrared image of the heat transfer process in Figure S8 in the Supporting Information. The anisotropic thermal properties are mainly attributed to the well-preserved alignment of the wood cells even after delignification and polymer infiltration. The anisotropic factor is calculated as ≈2 based on the ratio of the thermal conductivities in the axial and radial directions. Figure 4b also shows that our transparent wood has a smaller thermal conductivity (0.19 W m^{-1} K^{-1}) compared to glass (≈1 W m^{-1} K^{-1}), suggesting it has great potential for replacing glass windows and saving energy.

Moreover, we placed a regular glass slide (isotropic) and transparent wood (anisotropic) under a conductive heat source to further reveal the thermal management capabilities of the transparent wood (Figure 4c). The top surface of the sample was directly contacted with the conductive heat source using thermal paste, and after applying different temperatures ranging from 37 to 180 °C, we measured the stabilized backside temperatures of the samples via a K-type thermocouple (Figure 4d). When the heat source temperature is 65 °C, the backside temperature of the glass is 42 °C while the temperature of the transparent wood is only 31 °C (Figure S9, Supporting Information). These results show that our transparent wood yields a lower backside temperature under the same source temperature, which profits from the lower thermal conductivity in the radial direction as well as the preferred thermal dissipation in the axial direction due to its anisotropy.

Our transparent wood has outstanding performances in terms of high clarity, toughness, and thermal insulation as previously described, making it a promising candidate for glazing applications. To better evaluate the potential of this material for window applications, we conducted an energy modeling using EnergyPlus 8.2.0 software. Currently, the dominant technology for efficient windows is the double-pane insulated unit, in which air or other gases occupy the space between panes to provide additional thermal resistance. To validate the performance of our transparent wood, we constructed a model based on a double-pane transparent wood window system with standard air filling between the gap. The system was created via WINDOW 7.6 algorithm developed by Lawrence Berkeley National Laboratory (LBNL).[42] First, we confirmed the optical properties of single-pane transparent wood, including its weighted solar transmittance (T_{sol}), solar reflectance (R_{sol}), visible transmittance (T_{vis}), and visible reflectance (R_{vis}) of the single-pane transparent wood, which were calculated based the integration of the solar radiation at the earth's surface AM 1.5G spectrum covering a wide wavelength range of 280 nm to 2.5 µm (**Figure 5**a). Table S3 in the Supporting Information

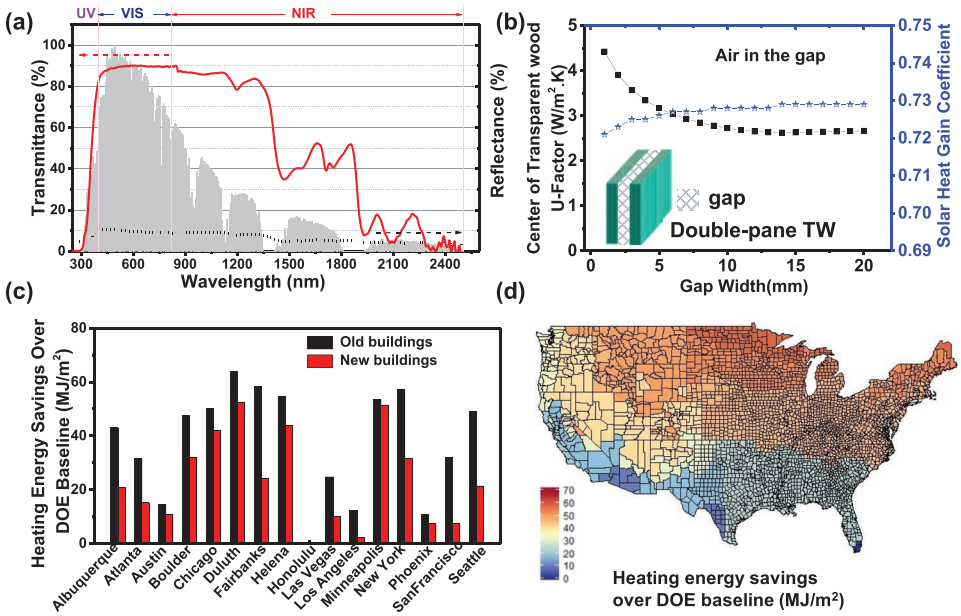

Figure 5. Energy savings model of double-pane transparent wood-based windows over the DOE baseline. a) Transmittance and reflectance of the single pane transparent wood. The gray area is the air mass normalized 1.5G solar radiation spectrum at the earth's surface with a wavelength range of 280 nm to 2.5 µm. b) The curve depicts the center *U*-factor and solar heat gain coefficient of the double-pane system based on two layers of the transparent wood as a function of different air thicknesses, which were calculated using the WINDOW7.6 algorithm developed by LBNL. c) Based on the Simple Window Model within EnergyPlus 8.2.0, the modeling results reveal that the 16 studied cities in the U.S. demonstrate heating energy saving potential over the DOE baseline during winter using double-pane transparent wood-based windows. d) The heating energy savings pattern for the continental U.S. over the DOE baseline.

summarizes all related variables of the single-pane transparent wood. Adapted from the LBNL Gap Library in the WINDOW 7.6 software,[43] air (ID: 1) was applied to fill between the double-pane transparent wood-based window model. The properties of the filling air are summarized in Table S4 in the Supporting Information. After applying all the information of the single-pane transparent wood with the air gap in the WINDOW 7.6 glazing system, the properties of the double-pane transparent wood were thus obtained, including its heat transfer coefficient (*U*-factor), solar heat gain coefficient (SHGC), and light transmittance (V_T), which were used to evaluate the performance and characteristics of the glazing. As depicted in Figure 5b, the center *U*-factor and SHGC of the double-pane transparent wood system are plotted (schematic illustration in Figure 5b) as a function of different air thicknesses. Then, we applied EnergyPlus 8.2.0 as a modeling tool to verify the heating energy consumption in cold weather using this transparent wood as a window material (see Discussion S1 in the Supporting Information). Based on statistical data provided by the Department of Energy (DOE) for 16 different cities in the U.S. in cold weather, we studied traditional, midrise-style apartment reference buildings, including older structures built prior to 1980 and newer ones built after 2004,[44] using double-pane transparent wood for the windows via the Simple Window Model applied in EnergyPlus 8.2.0. The energy modeling process establishes a baseline energy-consumption pattern for old and new buildings, then modifies the external windows' material properties based on the double-pane transparent wood's *U*-factor (2.93 W m^{-2} K^{-1}, at an air thickness of 7 mm), SHGC (0.727), and V_T (0.768) to predict a new energy-consumption pattern.

The chart in Figure 5c shows the total heating energy savings potential of the double-pane transparent wood-based windows over the DOE baseline energy consumed for the selected 16 U.S. cities. As the results demonstrate, using double-pane transparent wood windows led to an average energy savings of 38 and 23 MJ m^{-2} in old and new buildings per year over baseline, respectively. Specifically, cities usually experience extremely cold winters featured the highest heating energy saving potential, including Chicago (46 MJ m^{-2}), Duluth (58 MJ m^{-2}), Helena (49 MJ m^{-2}), Minneapolis (52 MJ m^{-2}), and New York (44.5 MJ m^{-2}). In Figure 5d, the continental U.S. map illustrates the potential improvement heating energy consumption using double-pane transparent wood-based windows for different cities compared to the standard baseline defined by the DOE. The graph shows higher heating energy savings potential toward the northern part of the country, where winter is colder. The relatively low thermal transmittance and *U*-factor, and relatively high solar heat gain of the double-pane transparent wood-based windows are responsible for the heating energy savings during the winter season. However, these thermal factors have a negative effect during the summer because they increase the energy consumption for cooling. Overall, transparent wood demonstrated a positive effect on the heating energy savings over the studied baseline model. Moreover, we also conducted a materials cost analysis for the transparent wood windows, which we estimated to be as low as \$2.513 m^{-2}, including all raw materials and treatment chemicals (Table S5, Supporting Information), which combined with the other optical, mechanical, and thermal characteristics suggest this energy-efficient material has the potential for practical applications in the built environment.

3. Conclusions

In conclusion, this work has demonstrated a high clarity, biodegradable transparent wood that can be assembled scalable with various superior properties, enabling this sustainable material to be potentially applied as a transparent, energy-saving building material. The transparent wood simultaneously features low haze (≈15%) and high transmittance (≈91%). Additionally, the transparent wood exhibits enhanced mechanical properties and low mass density, which can further eliminate the associated safety risks of glass windows. Moreover, it features good thermal resistance, with a low thermal conductivity of 0.19 W m^{-2} K^{-1} to enhance the energy efficiency compared to traditional glass windows. When assembled as a double-pane window with air filling the intervening gap, our transparent wood can provide an average energy savings over the DOE baseline by 38 and 23 MJ m^{-2} per year in old and new buildings, respectively. The results demonstrate that a scalable, high clarity, strong, and thermally insulated transparent wood may be a promising step toward the development of energy efficient building materials with many environmental and economic benefits.

4. Experimental Section

Materials and Chemicals: In this work, balsa wood (purchased from Specialized Balsa Wood, LLC, USA) was used to fabricate the transparent wood with density of 172 ± 12 kg m^{-3}. The 5% sodium hypochlorite (NaClO) solution (Laboratory-grade, Carolina) was applied to delignification. PVA (average M_w ≈ 85000–124000, 98–99% hydrolyzed) was purchased from Sigma-Aldrich. Deionized (DI) water was used throughout as a solvent.

Delignification Process: The natural balsa veneer slices were immersed directly into the commercial 5% NaClO solution at room temperature, followed by rinsing in DI water three times to remove any residual chemicals. The resulting wood samples were freeze dried to obtain the white wood slices.

Fabrication of the Transparent Wood: First, the PVA solution was prepared by dissolving the powder polymer in DI water at a concentration of 8 wt% at 90 °C. The dry white wood slice was placed in a plastic box and immersed in the PVA solution at a depth about more than 15 times of the wood thickness. The wood slice was then infiltrated by degassing the solution under 200 Pa. Finally, the box was placed in a hot oven at 60 °C to dry and solidify for about 48 h total. Finally, the obtained transparent wood was separated from the box.

Characterization: Tecan XEIA FEG SEM was used for characterizing the morphologies of the wood samples with gold coating. The two-step sulfuric acid hydrolysis method was applied for the composition content analysis according to previous research.[45] A UV–vis Spectrometer Lambda 35 (PerkinElmer, USA) equipped with an integrating sphere was utilized to measure all optical properties: transmittance, haze, and reflectance. A 532 nm (green) single mode laser DJ532-10 (Thorlabs, Inc.) was applied as the incoming light source with a spot size of ≈200 µm. The scattering light intensity distribution map of the transmitted light through the transparent wood was detected by a photodiode power sensor S-130 C from Thorlabs. The stress–strain measurements were processed via a Tinius Olsen H5KT testing machine and three specimens (totally dry, sustaining 0 RH) were measured to obtain the average results. The thermal performance measurements involved two forms: qualitative test for the thermal insulation performance under the conductive heating source and thermal conductivity measurements. A contact area of 4 mm × 4 mm was used for the applied conductive heat source, which was maintained in direct contact with a conductive thermal paste. A K-type gauge thermocouple was applied to test the backside temperatures of the samples while they reached a steady state.

Moisture Stability and Water Resistance Tests: The transparent wood (20 mm × 40 mm × 0.8 mm) with improved moisture stability was further developed. A thin layer of commercially available oil-based paint (Polyurethane, Minmax) was painted onto the transparent wood. After the painting was completely dry, the painted and nonpainted transparent wood samples were put into humidity chamber (LHS-150HC-II, set to 25 °C, 95% RH). As shown in Figure S10a in the Supporting Information, the thickness changes were further measured at regular intervals. The problem of thickness swelling could be dramatically improved for the painted transparent wood. Moreover, the stress–strain curves of nonpainted and painted transparent wood before and after exposure to humidity (95% RH) are illustrated in the Figure S10b in the Supporting Information. The results revealed that the mechanical properties of painted transparent wood remained almost unchanged after sustaining 95% RH for 150 h. In contrast, the tensile strength of nonpainted transparent wood decreased significantly after sustaining 95% RH for 150 h. Meanwhile, the water resistance of the painted transparent wood was greatly improved as shown in Figure S10c,d in the Supporting Information. After the painted and unpainted samples were immersed into DI water for 24 h at room temperature, respectively, the painted sample was shown to be more water resistant while the unpainted one (control sample) became swelled and curled.

Thermal Conductivity Measurement: Laser flash is a widely used transient method to determine the thermal diffusivities of bulk materials, which employs noncontact and nondestructive temperature sensing.[46,47] During the measurements, the instantaneous light was used as a heat source to heat the sample's front side, and an infrared detector was used to record the temperature response of the rear side. A very thin graphite coating was applied to both faces of the samples to act as an absorber on the front side and emitter on the rear side. With the assumption that the heat transfer is 1D, the thermal diffusivity α can be calculated using the following expression

$$\alpha = \frac{1.38d^2}{\pi^2 t_{1/2}} \tag{1}$$

where d is the thickness of the sample and $t_{1/2}$ is the time that it takes for the sample to heat to one half of the maximum temperature on the rear surface. The thermal conductivity k is then calculated by

$$k = \alpha \rho c_p \tag{2}$$

where α (mm^2 s^{-1}) is the measured thermal diffusivity, ρ is the density, and c_p is the heat capacity. In the measurements, a commercial Netzsch LFA 457 and Netzsch differential scanning calorimeter (DSC 204 F1_Phoenix) were used for the thermal diffusivity and heat capacity measurements, respectively.

Supporting Information

Supporting Information is available from the Wiley Online Library or from the author.

Acknowledgements

The authors acknowledge the support of the Maryland Nanocenter-AIM Lab, especially Dr. Rao and Dr. Liu. They acknowledge the support of the A. James & Alice B. Clark Foundation and the A. James School of Engineering at the University of Maryland.

Conflict of Interest

The authors declare no conflict of interest.

Author Contributions

R.M. and T.L. contributed equally to this work. L.H., R.M., and T.L. designed the experiments. R.M. fabricated the transparent wood and conducted SEM characterization. J.S. and D.D. were responsible for the energy model. R.Y. and X.Z. measured the thermal conductivity. Y.K. created the 3D illustrations. S.H. and T.L. performed optical measurements. C.C. revised the manuscript. W.G. conducted the mechanical measurements. J.Z. and W.X. carried out the wood composition measurements. L.H., R.M., and T.L. collectively wrote the paper. All authors commented on the final manuscript.

Keywords

building materials, energy efficiency, low haze, scalable, strong, thermal insulation, transparent wood

Received: September 10, 2019
Revised: October 19, 2019
Published online: November 18, 2019

[1] P. Nejat, F. Jomehzadeh, M. M. Taheri, M. Gohari, M. Z. Abd. Majid, *Renewable Sustainable Energy Rev.* **2015**, *43*, 843.
[2] D&R International Ltd, *2011 Buildings Energy Data Book*, U.S. Department of Energy **2012**.
[3] S. D. Rezaei, S. Shannigrahi, S. Ramakrishna, *Sol. Energy Mater. Sol. Cells* **2017**, *159*, 26.
[4] E. ARPA, https://arpae.energy.gov/sites/default/files/documents/files/SHIELD_ProgramOverview.pdf **2016**.
[5] D. E. Curcija Charlie, Investigator Principal, *Lawrence Berkeley National Laboratory-Windows and Envelope Materials Group* **2013**.
[6] Y. Li, Q. Fu, S. Yu, M. Yan, L. Berglund, *Biomacromolecules* **2016**, *17*, 1358.
[7] EPA U. S. *Environmental Protection Agency* **2011**.
[8] C. Cuevas, A. Fissore, N. Fonseca, *Energy Build.* **2010**, *42*, 1685.
[9] P. A. Fokaides, A. Kylili, S. A. Kalogirou, *Mater. Renewable Sustainable Energy* **2015**, *4*, 6.
[10] L. L. Fernandes, E. S. Lee, A. McNeil, J. C. Jonsson, T. Nouidui, X. Pang, S. Hoffmann, *Energy Build.* **2015**, *90*, 188.
[11] A. M. Nilsson, A. Roos, *Thin Solid Films* **2009**, *517*, 3173.
[12] C. Li, J. Tan, T.-T. Chow, Z. Qiu, *Energy Build.* **2015**, *102*, 129.
[13] M. Arıcı, H. Karabay, M. Kan, *Energy Build.* **2015**, *86*, 394.
[14] T. Li, M. Zhu, Z. Yang, J. Song, J. Dai, Y. Yao, W. Luo, G. Pastel, B. Yang, L. Hu, *Adv. Energy Mater.* **2016**, *6*, 1601122.
[15] M. Zhu, T. Li, C. S. Davis, Y. Yao, J. Dai, Y. Wang, F. AlQatari, J. W. Gilman, L. Hu, *Nano Energy* **2016**, *26*, 332.
[16] M. Zhu, J. Song, T. Li, A. Gong, Y. Wang, J. Dai, Y. Yao, W. Luo, D. Henderson, L. Hu, *Adv. Mater.* **2016**, *28*, 5181.
[17] Y. Li, S. Yu, J. G. C. Veinot, J. Linnros, L. Berglund, I. Sychugov, *Adv. Opt. Mater.* **2017**, *5*, 1600834.
[18] E. Vasileva, Y. Li, I. Sychugov, M. Mensi, L. Berglund, S. Popov, *Adv. Opt. Mater.* **2017**, *5*, 1700057.
[19] Y. Li, Q. Fu, X. Yang, L. Berglund, *Philos. Trans. R. Soc., A* **2018**, *376*, 20170182.
[20] W. Gan, S. Xiao, L. Gao, R. Gao, J. Li, X. Zhan, *ACS Sustainable Chem. Eng.* **2017**, *5*, 3855.
[21] Z. Yu, Y. Yao, J. Yao, L. Zhang, Z. Chen, Y. Gao, H. Luo, *J. Mater. Chem. A* **2017**, *5*, 6019.
[22] Y. Li, Q. Fu, R. Rojas, M. Yan, M. Lawoko, L. Berglund, *ChemSusChem* **2017**, *10*, 3445.
[23] J. Wang, C. Gao, Y. Zhang, Y. Wan, *Mater. Sci. Eng. C* **2010**, *30*, 214.
[24] Y. Li, M. Cheng, E. Jungstedt, B. Xu, L. Sun, L. Berglund, *ACS Sustainable Chem. Eng.* **2019**, *7*, 6061.
[25] Y. Li, X. Yang, Q. Fu, R. Rojas, M. Yan, L. A. Berglund, *J. Mater. Chem. A* **2017**, *6*, 1094.
[26] M. Borrega, P. Ahvenainen, R. Serimaa, L. Gibson, *Wood Sci. Technol.* **2015**, *49*, 403.
[27] P. Dashora, G. Gupta, *Polymer* **1996**, *37*, 231.
[28] M. Uwe, R. T. Manfred, S. Manfred, S. Melanie, Z. B. Harald, *J. Photochem. Photobiol., B* **2003**, *69*, 97.
[29] C. Jia, T. Li, C. Chen, J. Dai, I. M. Kierzewski, J. Song, Y. Li, C. Yang, C. Wang, L. Hu, *Nano Energy* **2017**, *36*, 366.
[30] N. Mbk, Z. Jahan, S. S. Berg, Ø. W. Gregersen, *Carbohydr. Polym.* **2017**, *177*, 258.
[31] A. K. Sonker, A. K. Teotia, A. Kumar, R. K. Nagarale, V. Verma, *Macromol. Chem. Phys.* **2017**, *218*, 1700130.
[32] J. Zhang, C. Li, C. Yu, X. Wang, Q. Li, H. Lu, Q. Zhang, J. Zhao, E. Songfeng, M. Hu, Y. Yao, *Compos. Sci. Technol.* **2019**, *169*, 167.
[33] S. Fink, *Holzforschung* **1992**, *46*, 403.
[34] A. Mandal, D. Chakrabarty, *J. Ind. Eng. Chem.* **2014**, *20*, 462.
[35] Z. Fang, H. Zhu, W. Bao, C. Preston, Z. Liu, J. Dai, Y. Li, L. Hu, *Energy Environ. Sci.* **2014**, *7*, 3313.
[36] H. Zhu, Z. Fang, Z. Wang, J. Dai, Y. Yao, F. Shen, C. Preston, W. Wu, P. Peng, N. Jang, Q. Yu, Z. Yu, L. Hu, *ACS Nano* **2016**, *10*, 1369.
[37] H. S. Yaddanapudi, N. Hickerson, S. Saini, A. Tiwari, *Vacuum* **2017**, *146*, 649.
[38] C. Boye, F. Preusser, T. Schaeffer, *WAAC Newsl.* **2010**, *32*, 13.
[39] N. X. Chen, J. H. Zhang, *Chin. J. Polym. Sci.* **2010**, *28*, 903.
[40] T. Rouxel, J. C. Sanglebœuf, *J. Non-Cryst. Solids* **2000**, *271*, 224.
[41] X. Zhao, C. Huang, Q. Liu, I. I. Smalyukh, R. Yang, *J. Appl. Phys.* **2018**, *123*, 085103.
[42] R. Mitchell, C. Kohler, D. Arasteh, *Lawrence Berkeley National Laboratory* **2003**.
[43] J. Apte, D. Arasteh, *Lawrence Berkeley National Laboratory* **2008**, 1.
[44] M. Deru, K. Field, D. Studer, K. Benne, B. Griffith, P. Torcellini, B. Liu, M. Halverson, D. Winiarski, M. Rosenberg, M. Yazdanian, J. Huang, D. Crawley, *National Renewable Energy Laboratory* **2011**, 1.
[45] X. Luo, R. Gleisner, S. Tian, J. Negron, W. Zhu, E. Horn, X. J. Pan, J. Y. Zhu, *Ind. Eng. Chem. Res.* **2010**, *49*, 8258.
[46] D. Zhao, X. Qian, X. Gu, S. A. Jajja, R. Yang, *J. Electron. Packag.* **2016**, *138*, 040802.
[47] X. Zhao, S. A. Mofid, M. R. Al Hulayel, G. W. Saxe, B. P. Jelle, R. Yang, *Appl. Therm. Eng.* **2019**, *160*, 114026.